Cellulose (2020) 27:6563–6576
https://doi.org/10.1007/s10570-020-03236-0

ORIGINAL RESEARCH

# UV-blocking, transparent and hazy cellulose nanopaper with superior strength based on varied components of poplar mechanical pulp

**Xinping Li · Xin Zhang · Shuangquan Yao · Hui Chang · Yaoyu Wang · Zhao Zhang**

Received: 17 January 2020 / Accepted: 13 May 2020 / Published online: 19 May 2020


**Abstract** The components of poplar mechanical pulp (PMP), including cellulose, hemicellulose, and lignin, were regulated through a drop-down synthesis method to prepare a series of mechanically superior raw, hemicellulose-containing (HNP), lignin-containing (LNP), and pure cellulose nanopaper (CNP). The effects of hemicellulose and lignin components on the transparency, haze, and mechanical properties were comprehensively investigated. Consequently, the resulting HNP and LNP combined high transparency (> 95%) and optical haze (> 76%) and possessed superior mechanical properties (182 and 148 MPa tensile strength). The residual lignin content (17.2–14.7 wt%) in LNP gave rise to efficient ultraviolet radiation blocking (∼ 100%) in the range of 200–320 nm. Moreover, HNP and LNP exhibited excellent flexibility and hydrophobicity and good thermal stability, which offered the potential for a wide range of applications in solar cells, light softening substrate, and light diffusers.

**Electronic supplementary material** The online version of this article (https://doi.org/10.1007/s10570-020-03236-0) contains supplementary material, which is available to authorized users.

X. Li · X. Zhang · Z. Zhang (✉)
College of Bioresources Chemical and Materials Engineering, National Demonstration Center for Experimental Light Chemistry Engineering Education, Shaanxi University of Science and Technology, Xi'an 710021, Shaanxi, People's Republic of China
e-mail: zhangzhaoqg@sust.edu.cn

S. Yao
Guangxi Key Laboratory of Clean Pulp and Papermaking and Pollution Control, College of Light Industry and Food Engineering, Guangxi University, Nanning 530004, People's Republic of China

H. Chang
College of Mechanical and Electrical Engineering, Shaanxi University of Science and Technology, Xi'an 710021, People's Republic of China

Y. Wang · Z. Zhang
College of Chemistry and Materials Science, Northwest University, Xi'an 710127, Shaanxi, People's Republic of China

Z. Zhang
State Key Laboratory of Pulp and Paper Engineering, South China University of Technology, Guangzhou 510640, People's Republic of China

## Graphic abstract

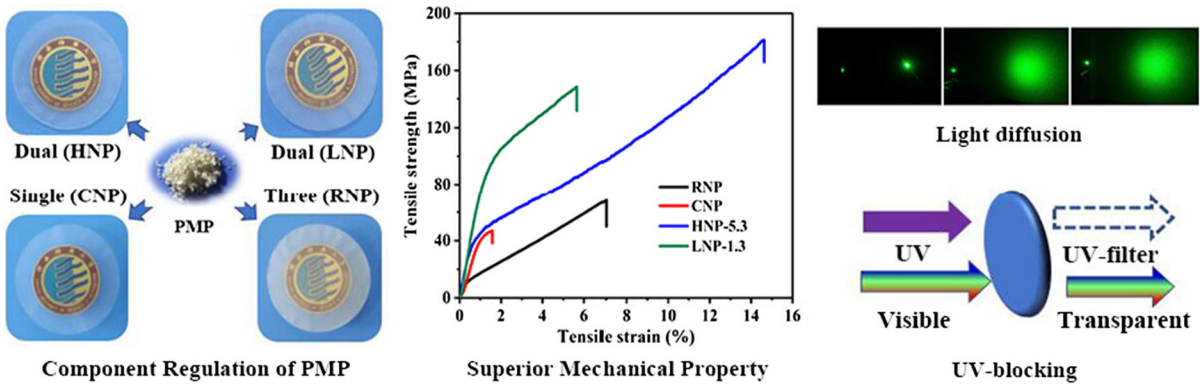


**Keywords** Component regulation · Superior mechanical strength · UV-blocking · Transparency and hazy · Poplar mechanical pulp

## Introduction

Cellulose nanopapers prepared from cellulose nanofibrils (CNFs) have emerged as interesting optical materials and have attracted intense attention due to their unique properties, including, transparency, haze, flexibility and low light absorption (Habibi. 2014; Klemm et al. 2011). Recently, optical transparency along with the presence of haze in cellulose nanopaper appears to offer intriguing attributes that are highly desirable for high-tech applications, such as in solar cells (Fang et al. 2014), organic light-emitting diodes (OLEDs; Mahpeykar et al. 2017), super capacitors (Leijonmarck et al. 2013), and flexible optoelectronics (Koga et al. 2014). Cellulose nanopaper applied in optoelectronics not only requires optical properties but also needs appropriate mechanical properties. Thus, it would be interesting to prepare superior mechanical cellulose nanopaper and overcome trade-off effects between haze and transparency.

Recently, transparency, optical haze and/or mechanical properties of cellulose nanopaper have been regulated via coordinating modification or grafting with petroleum-based polymers. Zhang et al. have constructed Zn-nanopaper by grafting of Zn(II)-terpyridine complex (Zn-tpy) into oxidized CNFs with controllable optical haze but poor mechanical properties (tensile strength at $\sim$ 70 MPa; Zhang et al. 2019a, b). Tang et al. have prepared cellulose nanopaper with haze and transparency using poly(-ethylene glycol) grafted CNFs via covalent bonding. The poly(ethylene glycol) as a "reinforcement" component endowed the nanopaper with excellent tensile strength (Tang et al. 2015). Chen et al. have developed a novel multifunctional nanopaper with high light transmittance (90.2%), high optical haze (46.5%) and excellent mechanical properties (103.7 MPa), which is composed of TEMPO-oxidized cellulose nanofibrils and polysiloxanes (Chen et al. 2018a). Zhang et al. have fabricated an optical haze ($\sim$ 100%) nanopaper based on a self-assembly process of tris(2 benzimidazolylmethyl) amine (NTB) [$(Tb(NTB)Cl_3$ and/or $Eu(NTB)Cl_3$] and TEMPO-oxidized cellulose nanofibrils (tCNFs). Unfortunately, the mechanical properties of this optical haze nanopaper are poor (15 MPa; Zhang et al. 2019a). However, the difficult preparation process and low repeatability of those coordinated or petroleum-based polymer modifications limit their further application in optoelectronics.

As is known, CNFs can be prepared from original cellulose fibers using physical and/or chemical methods (Chen et al. 2017; Henriksson et al. 2008; Mishra et al. 2018; Wagberg et al. 2008). The main chemical components of plant fibers are cellulose, hemicellulose, and lignin. Among these components, hemicellulose and lignin are important constituents of plant cell walls (Garcia Calvo-Flores and Dobado 2010; Svard et al. 2015). Lignin is covalently linked to cellulose and hemicellulose in plant fibers structures, providing structural rigidity and a physical barrier (Balakshin et al. 2011; Hu et al. 2016; Lawoko et al.

2005). In addition, hemicellulose has abundant hydroxyl groups distributed on its main and side chains, which are conducive of steric repulsions between the nanofibrils and can inhibit nanofibril agglomeration (Arola et al. 2013; Schroeter and Felix 2005). During the preparation process of cellulose nanopaper, air cavities are formed along with the destruction of hierarchical structure, thus creating heavy light scattering in the product. Amorphous component of the lignin and hemicellulose serve as reinforcement or cross-linking interactions to CNFs, resulting in cellulose nanopaper with excellent mechanical properties. Therefore, it is interesting to use natural-based polymer (lignin or hemicellulose) instead of petroleum-based polymers to prepare cellulose nanopaper, achieving the requirements of optical and mechanical properties for optoelectronics.

In this study, a series of pure, hemicellulose-containing, lignin-containing, and hemicellulose-lignin-containing CNFs was prepared from poplar mechanical pulp (PMP) using a mixed chemical and physical method. Further, a series of full component raw, dual component hemicellulose-containing, dual component lignin-containing, and single component cellulose nanopapers (RNP, HNP, LNP, and CNP, respectively) were prepared to fully explore the impact of each composition on nanopaper form and function. The performance of the present HNPs-n and LNPs-n exhibited superior mechanical properties (as high as 182 MPa) and achieved an anti-trade-off between transparency ($\sim$ 95%) and haze ($>$ 76%) performance. In addition, a certain content of lignin existed in these LNPs which gave rise to efficient UV-blocking ($\sim$ 100%). Thus, these high-strength nanopapers with high optical transparency, haze, and/or UV-blocking, could have important research value as a surface layer on an optical device as well as serve as a reinforcing structure in a polymer matrix composite.

## Experimental section

### Preparation of hemicellulose-containing nanopaper (HNP-17.8, 5.3, 3.9, and 2.3)

The PMP (the components included holocellulose, 76.2 wt%; hemicellulose, 18.4 wt%; lignin, 21.5 wt%; wax, 2.1 wt%), which were treated with sodium chlorite to obtain holocellulose. Further, four different hemicellulose content pulps (17.8, 5.3, 3.9, and 2.3 wt%) were obtained under different reaction times (0, 1, 2, and 3 h) using 10% NaOH at 50 °C (Farhat et al. 2017; Peng et al. 2009). All samples above were formulated to the same concentration (1 wt%) of fiber suspension with high-speed shearing; the preparation processes of HNPs were as follows. First, the suspension was homogenized at 30 MPa to form a uniform suspension and then 20 times at 60 MPa. For simplicity, the resulting nanofibrils were referred thereafter as hemicellulose-containing CNFs, termed H-CNF-17.8, H-CNF-5.3, H-CNF-3.9 and H-CNF-2.3, respectively. The H-CNFs were dried to constant mass and stirred at room temperature to ensure uniform nanofibril dispersion. HNP was prepared from the above H-CNF aqueous suspensions using vacuum filtration method. The wet cellulose nanopaper placed between smooth glass plates and allowed to dry at room temperature under a pressure of approximately 10 kg for 24 h. Finally, the resulting HNP products were labeled HNP-17.8, HNP-5.3, HNP-3.9 and HNP-2.3, respectively.

### Preparation of lignin-containing nanopaper (LNP-17.2, 14.7, 7.3, and 1.3)

The PMP was treated with NaOH (10%) to obtain lignin-containing cellulose. Further, four different lignin content pulps (17.2, 14.7, 7.3, and 1.3 wt%) were treated for various reaction times (0.5, 1, 2, and 4 h) using $NaClO_2$ at 50 °C. All samples were formulated to the same concentration (1 wt%) of fiber suspension with high-speed shearing, from which cellulose nanofibrils were obtained by high pressure homogenization. First, the suspension was homogenized at 30 MPa to form a uniform suspension and then 20 times at 60 MPa. For simplicity, the resulting nanofibrils were referred thereafter as lignin-containing CNFs, termed L-CNF-17.2, L-CNF-14.7, L-CNF-7.3 and L-CNF-1.3, respectively. The L-CNFs were dried to constant mass and stirred at room temperature in water to ensure uniform nanofibril dispersion. The preparation method of LNP nanopaper was the same as for that of HNP. Finally, the resulting LNPs were labeled LNP-17.2, LNP-14.7, LNP-7.3, and LNP-1.3.

Preparation of pure CNP

To obtain pure cellulose, PMP was successively treated with NaOH (10% by wt) for 3 h and then $NaClO_2$ for 4 h. The product was formulated into an aqueous fiber suspension at 1 wt% by high-speed shearing. The obtained pure cellulose suspension was homogenized at 30 MPa to form a uniform suspension and then 20 times at 60 MPa. The obtained C-CNFs were stirred at room temperature to ensure uniform nanofibril dispersion. CNP was prepared by the same method for HNP.

Preparation of RNP

PMP was formulated into an aqueous fiber suspension with a concentration of 1 wt% by high-speed shearing. The PMP suspension was homogenized at 30 MPa to form a uniform suspension and then 20 times at 60 MPa. The obtained R-CNFs were stirred at room temperature to ensure uniform dispersion of the nanofibrils. RNP was prepared in the same method as HNP.

## Results and discussion

Preparation and characterization of RNP, CNP, HNP-n (n = 17.8, 5.3, 3.9, and 2.3), and LNP-n (n = 17.2, 14.7, 7.3, and 1.3)

A series of pure, hemicellulose-containing, lignin-containing, and hemicellulose-lignin-containing CNFs was prepared from PMP using a mixed chemical andhigh-pressure homogenization method. The hemicellulose or lignin content of CNFs were controlled by the reaction time with NaOH or $NaClO_2$, producing a series of H-CNF (hemicellulose content: 17.8, 5.3, 3.9, and 2.3 wt%, termed H-CNF-17.8, H-CNF-5.3, H-CNF-3.9, and H-CNF-2.3 respectively) and L-CNF (lignin content: 17.2, 14.7, 7.3, and 1.3 wt%, termed L-CNF-17.2, L-CNF-14.7, L-CNF-7.3, and L-CNF-1.3, respectively). Subsequently, these CNF precursors were used to produce a series of nanopapers HNP-n (n = 17.8, 5.3, 3.9, or 2.3) and LNP-n (n = 17.2, 14.7, 7.3, or 1.3) via a simple vacuum filtration method (Scheme 1). For comparison, RNP and CNP were also prepared using a similar method.

Scanning electron microscope (SEM) images of H-CNFs (Fig. 1a) and L-CNFs (Li et al. 2019) clearly showed uniform nanofibril diameters and lengths on the order of microns after the freeze-drying process. R-CNFs were prepared from PMP via high-pressure homogenization, such that lignin and hemicellulose remained in the cellulose. As a result, the diameter of R-CNFs exhibited nonuniform distribution and exhibited a wide range, from 20 to 150 nm (Fig. S1), which was attributed to lignin and hemicellulose causing cross-linking of cellulose fibers. In contrast, lignin and hemicellulose removal would be conducive to its skeletal dispersion (Fig. S1), giving C-CNFs with high homogeneity and a network structure. The FT-IR spectrum of RNP, CNP, HNP-n (n = 17.8, 5.3, 3.9, or 2.3), and LNP-n (n = 17.2, 14.7, 7.3, or 1.3) showed that, compared with RNP and LNP-n, the peaks at 1600 $cm^{-1}$ (stretching vibrations of lignin phenyl C=C), 1505 (benzene skeleton vibrations), and 1458 $cm^{-1}$ (benzene vibrations and C–H asymmetric deformation in the lignin) attributed to CNP and HNP-n disappeared, which indicated that the lignin component was successfully removed from RNP and LNP (Fig. S2). Hydroxyl groups are strongly polar and hydroxyl associations easily occur between cellulose and hemicellulose molecules, such that a hydroxyl group association phenomenon occurs, which here caused the O–H stretching vibration absorption peak (3330 $cm^{-1}$) to become wide and strong in HNP-n (Ruiz et al. 2013). Analysis of XRD patterns of RNP, CNP, HNP-n and LNP-n showed that all these nanopapers maintained a typical crystal structure and still possessed the crystalline structure of cellulose I (Fig. S3). However, the crystallization index (CrI) of these nanopapers varied significantly (Table S1), with the CrI of RNP the lowest, at 28.8%. This result was attributed to a high content of amorphous hemicellulose and lignin. In contrast, after removing the hemicellulose and lignin amorphous components, CNP exhibited the highest CrI value (60.9%). For the HNP-n, HNP-2.3 had the highest CrI value, at 45.1%, compared to the CrI of the other HNP-n versions. The CrI value of LNP-n gradually increased with increased $NaClO_2$ reaction times. This further showed that the hemicellulose and lignin content in HNP and LNP were successfully controlled by adjusting the reaction times.

Atomic force microscopy (AFM) of HNP-n (n = 17.8, 5.3, 3.9 or 2.3) showed that total surface

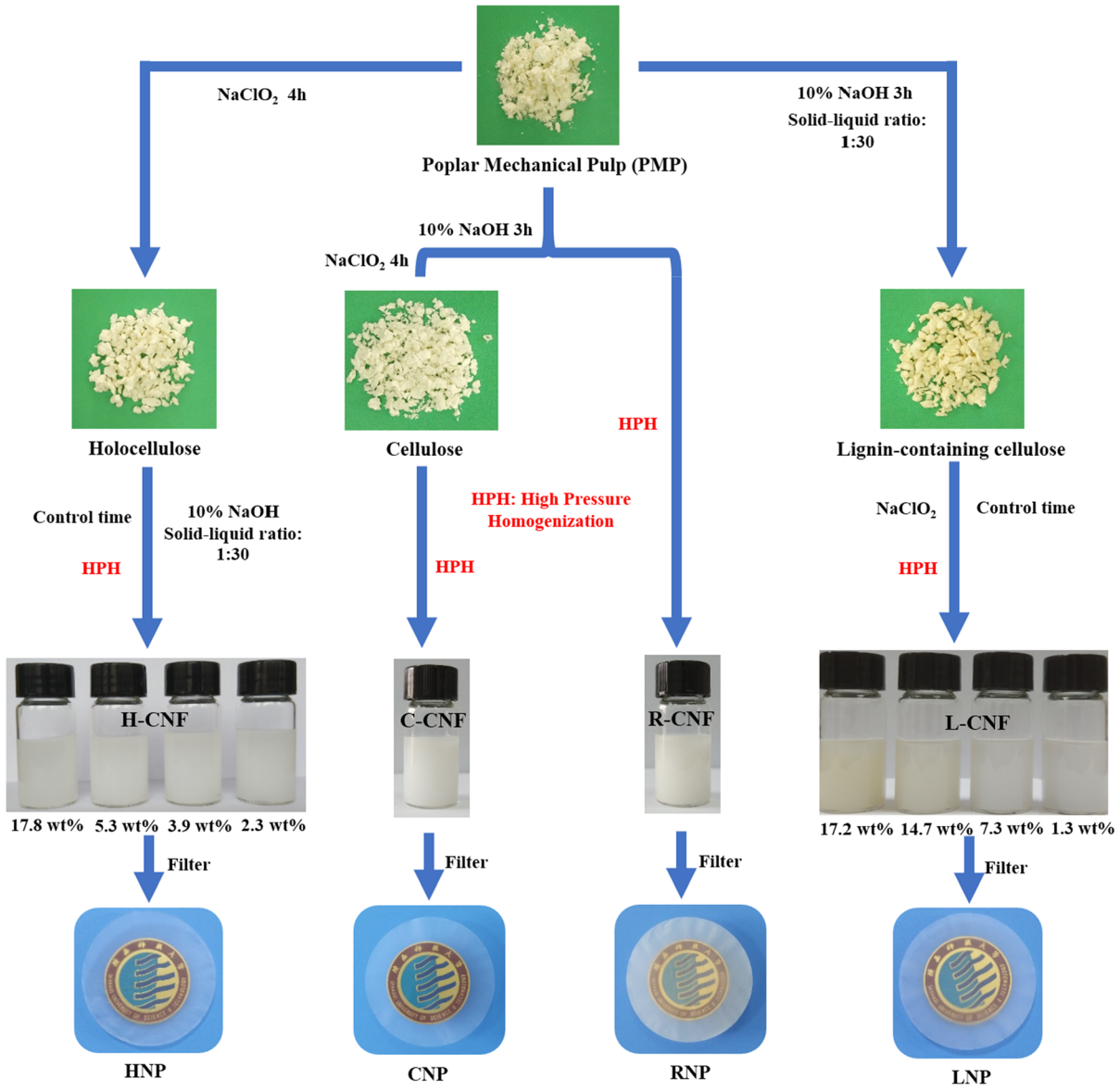


**Scheme 1** The reaction and prepared scheme for RNP, CNP, HNP-n (n = 17.8, 5.3, 3.9 and 2.3) and LNP-n (n = 17.2, 14.7, 7.3 and 1.3)

height ($S_z$) was the height between the highest peak and deepest valley. The $S_z$ of these HNP-n were 203, 359, 587 and 674 nm, respectively (Fig. 1b and Table 1). The root mean surface (RMS) roughness is an indicator of surface smoothness, which is related to fiber diameter and fiber agglomeration. HNP-17.8 with highest hemicellulose content showed the lowest RMS roughness value at 33.4 nm and the RMS roughness values of HNP-5.3, 3.9, and 2.3 were 59.5, 73.1, and 85.5 nm, respectively (Table 1). These results were because the presence of hemicellulose hindered fibril bundle formation and hemicellulose acted in cross-linking interactions and filled in the special gaps between the fibrils, thus improving nanopaper smoothness (Tarres et al. 2017; Yang et al. 2018).

The thermal stability of a substrate is very important for its actual application (Zhu et al. 2013). The thermal stability of RNP, CNP, HNP-n (n = 17.8, 5.3, and 2.3), and LNP-n (n = 17.2, 7.3, and 1.3) were

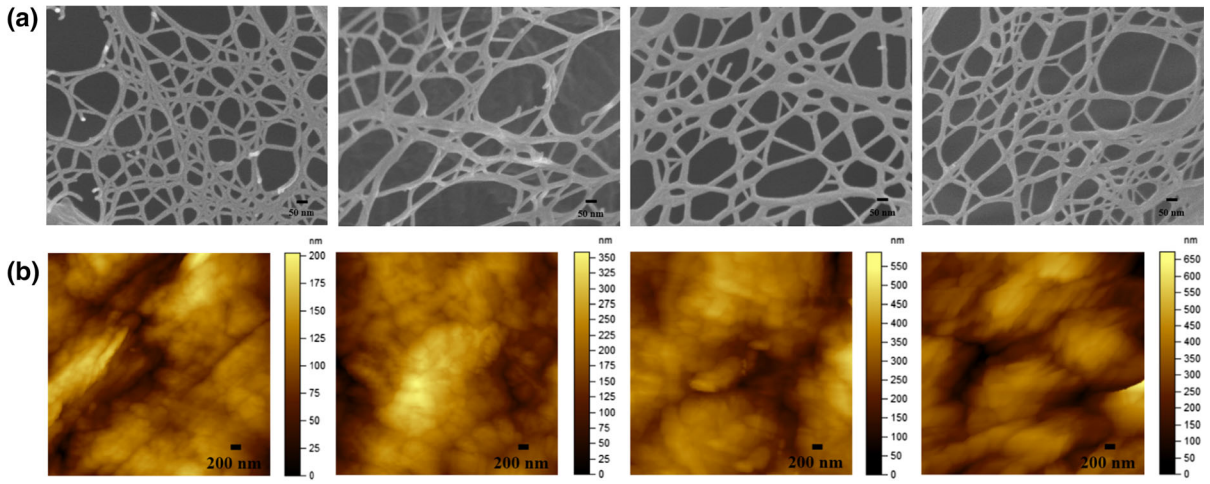


**Fig. 1** SEM images of different hemicellulose content nanofibrils: from left to right are H-CNF-17.8, 5.3, 3.9 and 2.3, respectively (**a**). AFM topographic images of the HNPs: from left to right are HNP-17.8, 5.3, 3.9 and 2.3, respectively (**b**)

**Table 1** The thickness and surface roughness properties of the HNP-n (n = 17.8, 5.3, 3.9 and 2.3)

| Sample | Thickness (μm) | RMS surface roughness (nm) | $S_z^a$ (nm) |
|---|---|---|---|
| HNP-17.8 | 17 ± 1 | 33.4 ± 1.0 | 203 |
| HNP-5.3 | 17 ± 1 | 59.5 ± 1.6 | 359 |
| HNP-3.9 | 18 ± 1 | 73.1 ± 2.2 | 587 |
| HNP-2.3 | 15 ± 1 | 85.5 ± 4.8 | 674 |

*RMS* Root mean square

[a]Total height of the surface

investigated using thermogravimetric analysis (TGA) under a nitrogen atmosphere (Fig. S4). As is known, thermal stability is affected by the crystalline state and particle size. Here, the amorphous component of lignin and hemicellulose depressed the CrI value of LNP and HNP, which was explained by the increased lignin or hemicellulose content of LNP and HNP causing thermal stability to decrease. Therefore, the excellent thermal stability ($T_{max}$ = 345 °C) of CNP was contributed by its high crystallinity. The RNP with the highest $T_{max}$ (355.4 °C, Table S2) was attributed to R-CNF in the RNP having large particle sizes (Fig. S1). For HNP-n, HNP-2.3 had the highest initial degradation temperature of 244.4 °C and a maximum weight loss temperature of 350 °C, compared to the other two HNP-n (n = 17.8 or 5.3, Table S2). Through delignification, the $T_{onset}$ (210.5–238.1 °C) and $T_{max}$ (331.2–337.2 °C) of LNP-n (n = 17.2, 7.3, and 1.3) showed an increasing trend (Table S2). This indicated that residual hemicellulose and lignin had a weak negative effect on nanopaper thermal stability.

The presence of hemicellulose was beneficial for improving HNP hydrophobicity. As expected here, the water contact angle (WCA) of these nanopapers decreased from 77.7° to 28.2° as the hemicellulose content decreased from 17.8 to 2.3 wt% (Fig. S5a). This further indicated the ability to control the hemicellulose content in the resulting HNP via control of the hemicellulose/NaOH reaction. The reason for the observed enhanced hydrophobicity was attributed to hemicellulose bound to hydroxyl groups on cellulose surfaces and the presence of hydrophobic xylan, which hindered hydrogen bond formation between cellulose and water and produced hydrophobicity (Fukuzumi et al. 2009; Gu and Hsieh 2015). Similarly, lignin was a hydrophobic component (Rojo et al. 2015; Spence et al. 2010), such that the WCA gradually

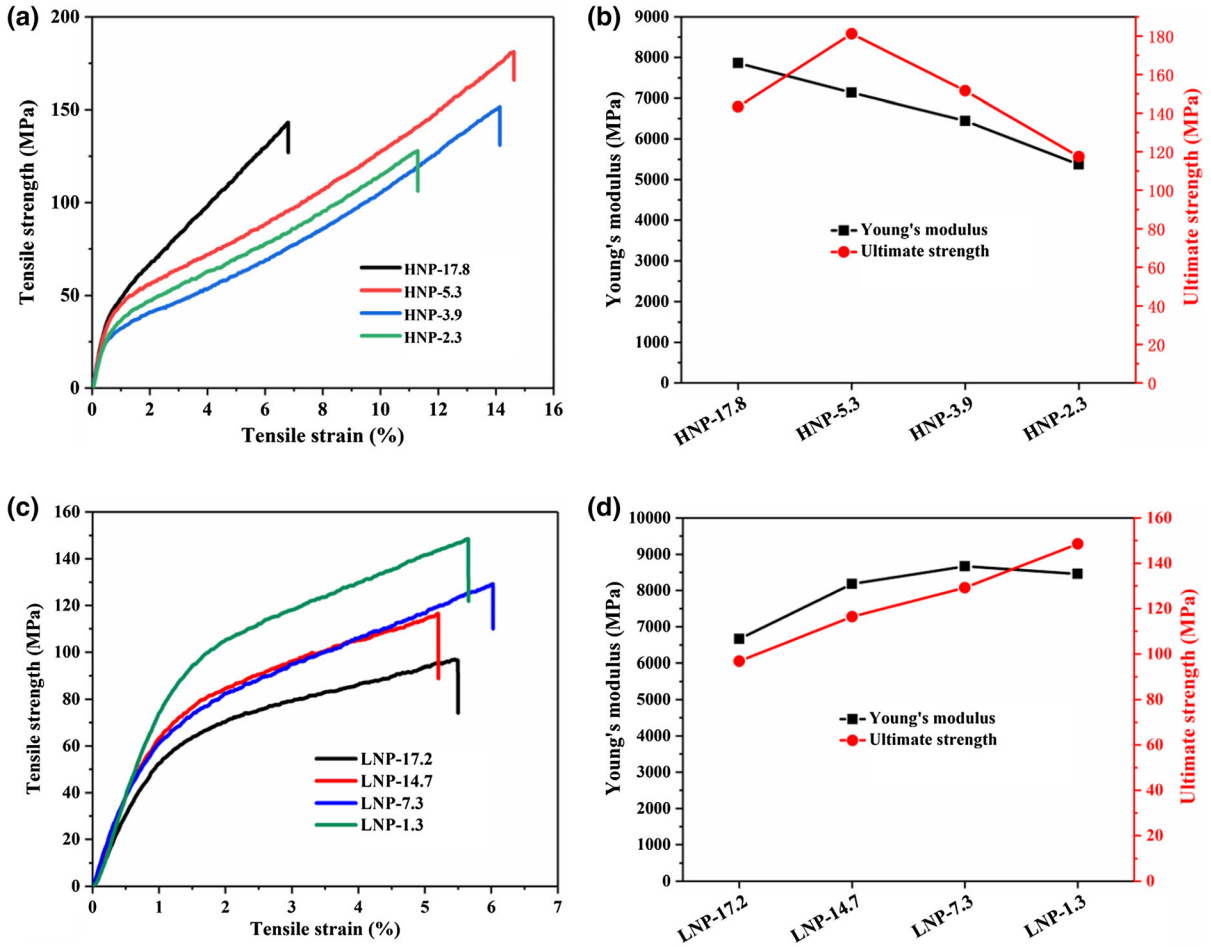


**Fig. 2** Mechanical properties of different hemicellulose or lignin content nanopapers: Tensile strength verus tensile strain curves (**a**) and (**c**), Young's modulus and ultimate strength (**b**) and (**d**)

decreased from 83.1° to 42.3° as lignin content decreased from 17.2 to 1.3 wt% (Li et al. 2019). Normally, CNP had lower hydrophobicity (WCA, 33.2°) due to C-CNF surfaces being rich in hydroxyl groups (Fig. S5b). It was noteworthy that RNP had a large amount of hydrophobic content (lignin and hemicellulose), but the WCA was 42.6° (Fig. S5c). Because of the high content of lignin and hemicellulose, nonuniform R-CNF formed a nanopaper with a fluffy state (with induced capillarity, Fig. S6j). In contrast, the uniformity of H-CNF and L-CNF endowed HNP and LNP with densely packed structure, thus achieving good hydrophobicity (Fig. S6a–h).

Superior mechanical properties of HNP-n (n = 17.8, 5.3, 3.9, and 2.3) and LNP-n (n = 17.2, 14.7, 7.3, and 1.3)

CNF as nanoscale fibers have a small diameter (< 100 nm), lengths of several microns, large specific surface areas, and produce a natural film with outstanding mechanical properties and flexibility. H-CNF and L-CNF have important research value as a reinforcing structure in polymer matrix composites and flexible optoelectronic devices. Compared with a traditional polymer-doped or chemical-modification method, a drop-down method was used here to prepare superior mechanical cellulose nanopapers. H-CNF-n (n = 17.8, 5.3, 3.9, and 2.3) and L-CNF-n (n = 17.2, 14.7, 7.3, and 1.3) exhibited good dispersibility in aqueous solution after high-pressure homogenization

(Scheme 1). Well-dispersed CNF and uniform nanosize helped form dense structures (Figs. S6a–h), endowing HNP and LNP with excellent mechanical performance. Different hemicellulose content nanopapers had similar thickness (Table 1). The tensile strengths of HNP-n were 143.3, 181.2, 151.6, and 117.5 MPa, respectively (Fig. 2a), with corresponding Young's moduli of 7861.7, 7135.6, 6443.6, and 5374.8 MPa, respectively (Fig. 2b). As the hemicellulose content (2.3 to 5.3 wt%) gradually increased, HNP tensile strength was enhanced from 117.5 to 181.2 MPa. Moreover, the tensile strain showed the same growth trend (11.3–14.6%), indicating that HNP-2.3–5.3 exhibited excellent toughness. A certain content of hemicellulose contributed to fibril structure and the bonding force between fibrils during the nanopaper formation process, thus improving the nanopaper mechanical properties, so-called "reinforcing" properties (Yang et al. 2018). However, the excessive hemicellulose content of HNP-17.8 resulted in poor tensile strength (143.3 MPa), which were attributed to low CrI (Table S1) and inhibited hydrogen bond formation between nanofibrils in the nanopaper. The thickness of cellulose nanopapers with different lignin content are shown in Table S3. As the lignin content decreased, the tensile strength and Young's modulus (tensile strengths of LNP-17.2–1.3 were at 96.8, 116.5, 129.2, and 148.6 MPa; Fig. 2c; and corresponding Young's moduli at 6664.8, 8182.5, 8665.7, and 8460.2 MPa, respectively; Fig. 2d) of LNP increase gradually. High residual lignin was found to interfere with the formation of intermolecular hydrogen bonds between fibers (Bian et al. 2018; Wang et al. 2018). Therefore, the mechanical properties of the nanopaper decreased significantly. In addition, the mechanical properties of the RNP was examined and the tensile strength found to be as low as 68.4 MPa as expected (Fig. S7). The cause of this phenomenon was explained as the non-uniformity and large size of R-CNF (Fig. S6j, red mark). Although the fracture surface of pure cellulose nanopaper showed a dense structure (Fig. S6i), pure cellulose nanopaper (without hemicellulose and lignin) exhibited lower tensile strength (46.7 MPa, Fig. S7) and toughness, which was lower than the relative values of LNP-n and HNP-n. This undesirable result was mainly due to the

**Fig. 3** Photo showing transparency and flexibility of nanopaper (**a**). UV transmission spectra of RNP, CNP, HNP-n (n = 17.8, 5.3, 3.9 and 2.3), and LNP-n (n = 17.2, 14.7, 7.3 and 1.3) (**b**, **d**). Optical haze of RNP, CNP, HNP-n (n = 17.8, 5.3, 3.9 and 2.3), and LNP-n (n = 17.2, 14.7, 7.3 and 1.3) (**c**, **e**). Photo shown light scattering effect of a laser passing through petroleum-based plastics film (**f**), HNP-17.8 (**g**) and LNP-17.2 (**h**)

**Table 2** Comparison of mechanical properties of various cellulose nanopapers

| Materials | Tensile strength (MPa) | References |
|---|---|---|
| HNP-5.3 | 182 | This work |
| LNP-1.3 | 148 | This work |
| L-CNF films | 22.6 | Chen et al. (2018b) |
| ACNF and OCNF films | 23.4 | Hu et al. (2016) |
| NFC film | 25.1 | Zhang et al. (2017) |
| BEP nanopaper | 30.4 | Malucelli et al. (2018) |
| TCCNP | 30.8 | Zhang et al. (2018) |
| Corn straw CNF films | 57.7 | Xu et al. (2018) |
| CNF films | 70.98 | Velasquez-Cock et al. (2016) |
| High residual lignin nanofibril film | 78 | Nair and Yan (2015) |
| TMP-L-CNF films | 85.6 | Horseman et al. (2017) |
| TOCN film | 92 | Yang et al. (2019) |
| L-CNF films | 115 | Bian et al. (2018) |
| CNF nanopaper | 330 | Galland et al. (2015) |

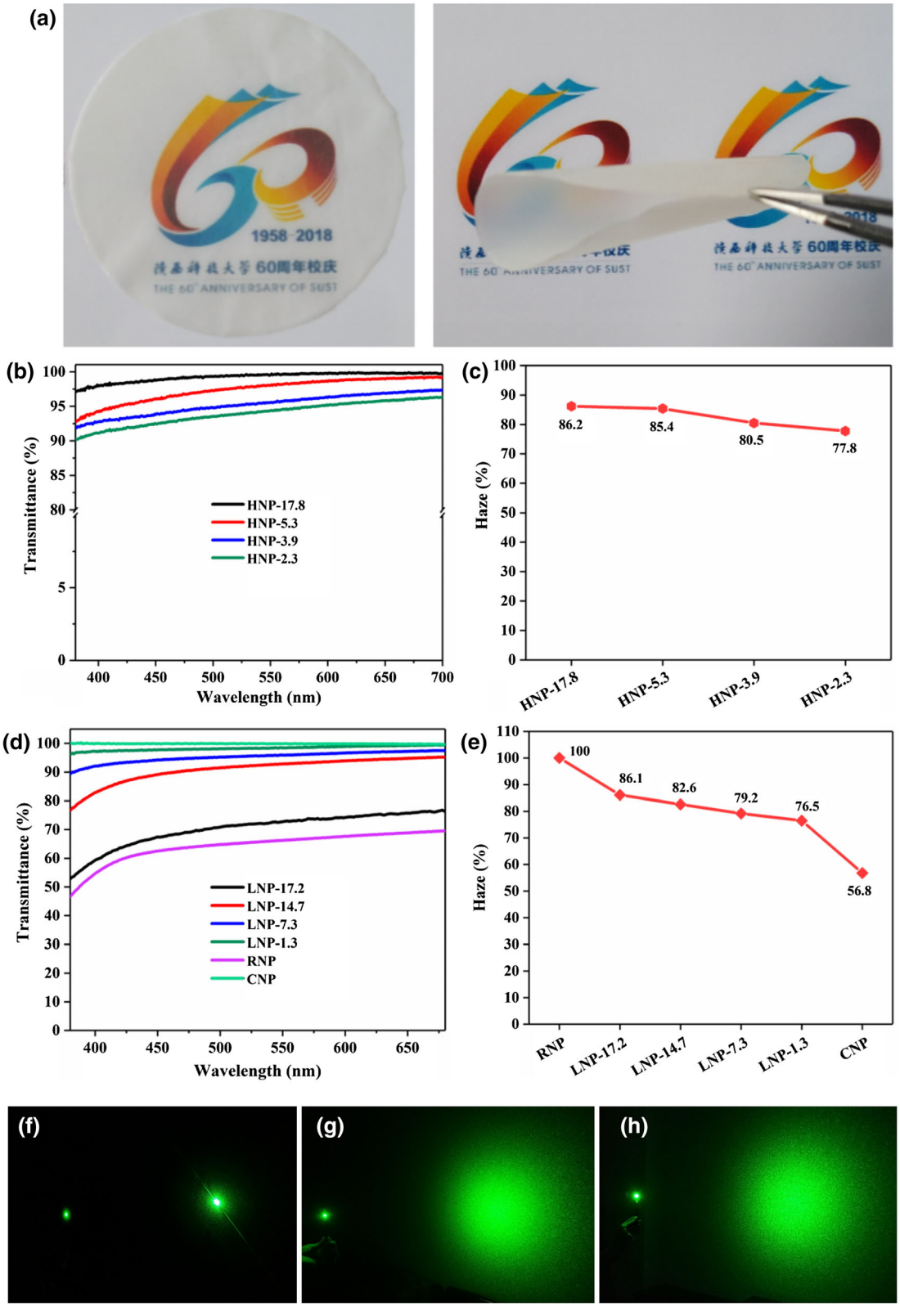
(a)
1958-2018
陕西科技大学 60周年校庆
THE 60TH ANNIVERSARY OF SUST
(b)
Transmittance (%)
Wavelength (nm)
HNP-17.8
HNP-5.3
HNP-3.9
HNP-2.3
(c)
Haze (%)
86.2
85.4
80.5
77.8
HNP-17.8
HNP-5.3
HNP-3.9
HNP-2.3
(d)
Transmittance (%)
Wavelength (nm)
LNP-17.2
LNP-14.7
LNP-7.3
LNP-1.3
RNP
CNP
(e)
Haze (%)
100
86.1
82.6
79.2
76.5
56.8
RNP
LNP-17.2
LNP-14.7
LNP-7.3
LNP-1.3
CNP
(f)
(g)
(h)

absence of hemicellulose and lignin. Therefore, a small amount of hemicellulose and/or lignin appeared to promote stress transfer between nanofibrils, thereby improving nanopaper mechanical properties (Ferrer et al. 2012; Rojo et al. 2015). These phenomena indicated that the content of noncellulosic components (mainly hemicellulose and lignin) as plant fibers were particularly important for nanopaper mechanical properties. The mechanical properties of various cellulose nanopapers indicated that these HNP-5.3 and LNP-1.3 possessed superior mechanical properties (Table 2).

### Light transparency and optical haze performance of RNP, CNP, HNP-n (n = 17.8, 5.3, 3.9, and 2.3), and LNP-n (n = 17.2, 14.7, 7.3, and 1.3)

Transparency and optical haze are important optical parameters for the functioning of optoelectronic devices, such as in light diffusers, OLEDs, and solar cells (Fang et al. 2014). To our knowledge, CNF paper usually possesses high transmittance (90%) and low optical haze, from 20 to 60%, with the latter value mainly dependent on the morphology or nanosize particles in the structure. It is difficult to eliminate 'trade off' effects between transparency and haze. Here, when the nanopaper directly covered a background picture, the logo behind the nanopaper was clearly seen (Fig. 3a). However, with the nanopaper a certain distance from the background picture, the logo was obscured, which was attributed to haze-induced light scattering. In addition, the nanopaper could be curled and folded, which indicated that nanopaper had good flexibility. As the hemicellulose content increased, the HNP-n (n = 17.8, 5.3, 3.9 and 2.3) light transmission increased (> 90%, in the visible light region; Fig. 3b) and the optical haze at 77.8–86.2% (Fig. 3c), thus achieving an anti-trade-off between transparency and haze performance. Surface light scattering might have prevented light transmission through the paper and backscattering also induced some light energy loss. It was interesting that HNPs had smooth surfaces (33.4–85.5 nm), which allowed low surface light scattering as well as high transparency (> 90%). Notably, with increased hemicellulose content, transparency slightly increased, which was attributed to low back-scattering caused by the low RMS roughness of this high hemicellulose-content nanopaper. For LNP-n (n = 14.7, 7.3, or 1.3), all exhibited excellent light transparency and optical haze (> 80 and > 76%, Fig. 3d and e, respectively). Notably, with variations in lignin or hemicellulose content, the same trend was observed for optical haze changes of LNP and HNP. However, the influences of lignin and hemicellulose on nanopaper optical haze were different. For HNP, hemicellulose has had a refractive index similar to cellulose (Niskanen et al. 2019; de Vasconcelos et al. 2015) and also filled special air voids, such that both contributed to decreasing the optical haze. For LNP, the increased optical haze induced by lignin was explained because lignin and cellulose had different refractive indices (Nemoto et al. 2010; Niskanen et al. 2019). As expected, CNP exhibited superior transparency, but the optical haze was lower (100 and 56.8%, Fig. 3d, e, respectively), which had the smallest target area through the green laser (Fig. S8b). Petroleum-based plastics are known to usually have high light transparency but low haze. To visualize the haze-induced light scattering behavior of HNP-17.8, LNP-17.2, or a petroleum-based plastic, a green laser light was passed through a nanopaper or film, producing variations in lit areas on a target screen. The plastic film caused little light scattering, producing the expected small radius light target spot after transmittance through the plastic (Fig. 3f). In contrast, the HNP-17.8 and LNP-17.2 showed greatly scattered green light and produced a larger and more homogeneous illuminated area on the target (Fig. 3g, h, respectively). Although RNP exhibited the highest optical haze, at 100%, and light scatting behaviors (Figs. 3e and S8a, respectively), the light transparency was only 65% (Fig. 3d). This was attributed to nonuniform nanosized particles (especially for large CNF particles) causing RNP with rough surfaces. More importantly, HNP-17.8 and LNP-1.3 exhibited > 95% light transparency and excellent optical haze (86.2 and 76.5%, respectively), in comparison to previously reported optical haze cellulose nanopapers (Table 3). The transparency and haze optical properties of HNP and LNP indicated that these materials had great application potential in

**Table 3** Comparison of optical properties of various cellulose nanopapers

| Materials | Transmittance (%) | Haze (%) | References |
|---|---|---|---|
| HNP-17.8 | > 95 | > 86 | This study |
| LNP-1.3 | > 95 | > 76 | This study |
| Holocellulose paper | 55 | 80 | Yang et al. (2018) |
| TOCNs/TOWFs-C film | 85 | 62 | Yang et al. (2019) |
| Nanopaper | 89 | 9 | Zhang et al. (2019b) |
| Hazy transparent nanopaper | 89–92 | 27–87 | Hsieh et al. (2017) |
| All cellulose composite film | 90 | 82 | Hu et al. (2018) |
| TEMPO nanopaper | 90.5 | 1.21 | Yagyu et al. (2015) |
| Super-clear nanopaper | 91 | 1.4 | Tao et al. (2017) |
| Transparent hybrid paper | 91.5 | 70 | Fang et al. (2013) |
| Transparent nanopaper | 92 | 41 | Chen et al. (2015) |
| Nanopaper | 93 | 50 | Zhu et al. (2013) |

paper-based anti-reflective materials, such as in photovoltaics and OLEDs (Ha et al. 2018).

### RNP and LNP-n (n = 17.2, 14.7, 7.3, and 1.3) for UV-blocking

The cumulative impact of solar UV rays acting on human skin can cause dermatitis or skin cancer (Juzeniene et al. 2011). The present LNPs were used as UV-filters for UV protection evaluation. These LNPs showed excellent UV-absorption ability, at > 80%, with absorption mainly ranging from 200 to 320 nm (Fig. 4a). Although LNP-17.2 and LNP-14.7 had different lignin contents, both exhibited similar UV-blocking ability (~ 100%; Li et al. 2019). Usually, a compound with π–π conjugate structures possesses unique UV-blocking ability. Lignin possesses many UV-absorbing functional groups, such as phenols and ketones, leading to excellent UV-absorption properties (Sadeghifar et al. 2017). The UV-blocking mechanism of lignin-containing nanopaper was explained as the transition of electrons (π–π*, n–σ* and n–π*) in lignin molecules (Nguyen et al. 2013). As biomass-derived materials, cellulose and hemicellulose are totally without UV-absorption capability in the 250–320 nm range and, thus, the observed UV-blocking was attributed to residual lignin content in LNP. The UV-blocking ability of LNP was positively correlated with lignin content, such that increased lignin content, from 1.3 to 17.2 wt%, resulted in UV-blocking enhancement from 80 to 100% (Li et al. 2019). Based on UV wavelengths, UV light is divided into UVA, UVB, and UVC (320–400, 275–320, and 200–275 nm, respectively). LNP had the maximum absorption peak located at 285 nm, which was typical of a UVB filter. Irradiation-time dependent UV–Vis spectra showed that LNP-1.3 had high photo-stability, with measurements every 30 min for 3 h (Fig. 4b). For CNP, and LNP, lignin was selectively removed to further clarify the reason for UV-blocking in LNP-n (n = 17.2, 14.7, 7.3, and 1.3). The UV-blocking property of nanopaper was further explored by studying the absorption and emission spectra of a Europium complex [$EuL_3Na_3$] ($H_2L$ = pyridine-2,6-dicarboxylic acid, Fig S9) were studied. This complex was confirmed by the observed range-broadening of in 200–300 nm UV-absorption. Under photo excitation at 254 nm, europium complex emitted strong pure red light of the $Eu^{3+}$ ion due to transitions from the emitting level ($^5D_0$) to the ground multiple $^7F_J$ (J = 0, 1, 2, 3, and 4; Fig. S10). As expected, the europium complex was lit up under a 254 nm UV lamp irradiation (Fig. 4c), but there were extremely weak emissions after adding RNP or LNP (Fig. 4d, e, respectively) between the europium complex solution and UV lamp. This indicated that RNP or LNP blocked UV light (254 nm) efficiently. However, after removing the lignin and hemicellulose components, CNP did not totally block UV light and allowed the europium complex solution with strong red emissions (Fig. 4f). Such high-efficiency UV-blocking and visible transparency LNP offered broad application prospects in the field of flexible optoelectronics (Zhang et al. 2019b).

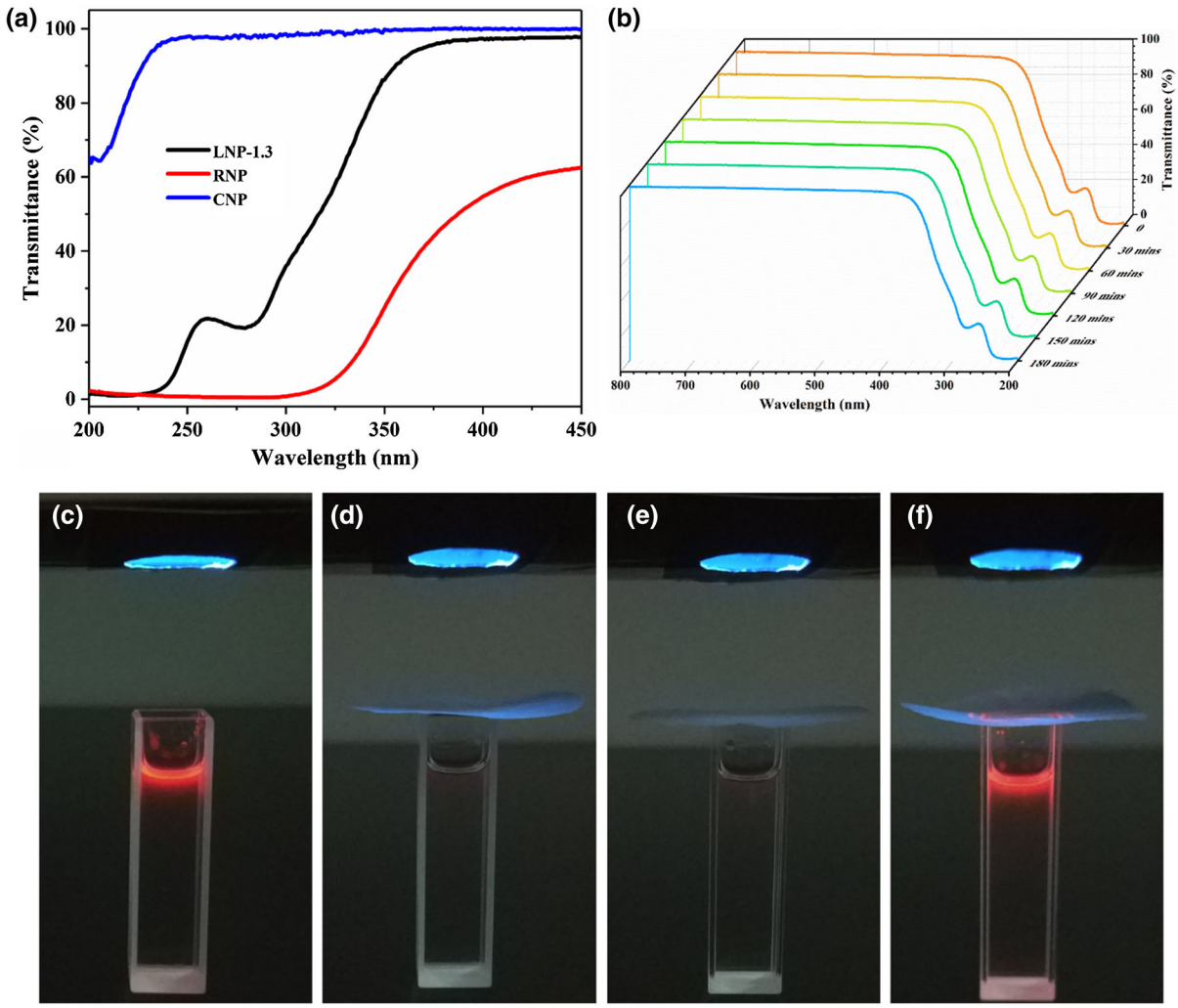


**Fig. 4** UV transmission curves of RNP, CNP and LNP-1.3 (**a**). UV transmission spectra of LNP-1.3 every 30 min (**b**). Photos of a glass vial containing europium complex [$EuL_3Na_3$] ($H_2$-L = pyridine-2,6-dicarboxylic acid) fluorescing under the illumination of a λ = 254 nm UV lamp (**c**), and fluorescence of the glass vial being excited when the UV lamp passes through RNP (**d**), LNP-17.2 (**e**) and CNP (**f**)

## Conclusions

In this study, a drop-down method was used to regulate PMP composition and to prepare mechanically superior nanopapers, achieving an anti-trade-off between transparency and haze performance and high efficiency UV-blocking. The results showed that the lignin and hemicellulose component distributions in these nanopapers had significant effects on light transparency, optical haze, and mechanical properties. Both LNP-1.3 and HNP-17.8 exhibited ultrahigh optical transparency (> 95%) and haze (> 76%). Interestingly, the performance of RNP and CNP in terms of the anti-trade-off of optical transparency and haze was disappointing. In addition, the residual lignin content (17.2–14.7 wt%) in LNP gave rise to efficient UV-blocking (∼ 100%) in the range of 200–320 nm. Overall, LNP-1.3 and HNP-5.3 were demonstrated here, confirmed to have high-strength (148 and 182 MPa tensile strength, respectively), light transparency, optical haze, and/or UV-blocking, such that these nanopapers have potential applications in UV-resistance, light softening substrate, and light diffusors.

**Acknowledgments** This work was supported by National Natural Science Foundation of China (21703131, 31370578), Doctoral Scientific Research Foundation of Shaanxi University of Science and Technology (2016BJ-40), State Key Laboratory of Pulp and Paper Engineering, South China University of Technology (201821), Special Research Fund by Shaanxi Provincial Department of Education (18JK0122), Chinese Postdoctoral Science Foundation (2018M643707), Natural Science Basic Research Plan in Shaanxi Province of China (2019JQ-516), Guangxi Key Laboratory of Clean Pulp and Papermaking and Pollution Control, College of Light Industry and Food Engineering, Guangxi University (2019KF18, 2019KF33).

## References

Arola S, Malho JM, Laaksonen P, Lille M, Linder MB (2013) The role of hemicellulose in nanofibrillated cellulose networks. Soft Matter 9:1319–1326

Balakshin M, Capanema E, Gracz H, Chang HM, Jameel H (2011) Quantification of lignin-carbohydrate linkages with high-resolution NMR spectroscopy. Planta 233:1097–1110

Bian H, Gao Y, Wang R, Liu Z, Wu W, Dai H (2018) Contribution of lignin to the surface structure and physical performance of cellulose nanofibrils film. Cellulose 25:1309–1318

Chen J, Han X, Fang Z, Cheng F, Zhao B, Lu P, Li J, Dai J, Lacey S, Elspas R, Jiang Y, Liu D, Hu L (2015) Rapid dissolving-debonding strategy for optically transparent paper production. Sci Rep 5:17705

Chen Y, Fan D, Han Y, Li G, Wang S (2017) Length-controlled cellulose nanofibrils produced using enzyme pretreatment and grinding. Cellulose 24:5431–5442

Chen S, Song Y, Xu F (2018a) Highly transparent and hazy cellulose nanopaper simultaneously with a self-cleaning superhydrophobic surface. ACS Sustain Chem Eng 6:5173–5181

Chen Y, Fan D, Han Y, Lyu S, Lu Y, Li G, Jiang F, Wang S (2018b) Effect of high residual lignin on the properties of cellulose nanofibrils/films. Cellulose 25:6421–6431

de Vasconcelos S, Moutta RD, Bon EPD, Cammarota MC, Ferreira-Leitao VS (2015) Fermentative biohydrogen production using hemicellulose fractions: analytical validation for C5 and C6-sugars, acids and inhibitors by HPLC. Int J Hydrogen Energy 40:13888–13900

Fang Z, Zhu H, Preston C, Han X, Li Y, Lee S, Chai X, Chen G, Hu L (2013) Highly transparent and writable wood all-cellulose hybrid nanostructured paper. J Mater Chem C 1:6191–6197

Fang Z, Zhu H, Yuan Y, Ha D, Zhu S, Preston C, Chen Q, Li Y, Han X, Lee S, Chen G, Li T, Munday J, Huang J, Hu L (2014) Novel nanostructured paper with ultrahigh transparency and ultrahigh haze for solar cells. Nano Lett 14:765–773

Farhat W, Venditti R, Quick A, Taha M, Mignard N, Becquart F, Ayoub A (2017) Hemicellulose extraction and characterization for applications in paper coatings and adhesives. Ind Crops Prod 107:370–377

Ferrer A, Quintana E, Filpponen I, Solala I, Vidal T, Rodriguez A, Laine J, Rojas OJ (2012) Effect of residual lignin and heteropolysaccharides in nanofibrillar cellulose and nanopaper from wood fibers. Cellulose 19:2179–2193

Fukuzumi H, Saito T, Wata T, Kumamoto Y, Isogai A (2009) Transparent and high gas barrier films of cellulose nanofibers prepared by TEMPO-mediated oxidation. Biomacromol 10:162–165

Galland S, Berthold F, Prakobna K, Berglund LA (2015) Holocellulose nanofibers of high molar mass and small diameter for high-strength nanopaper. Biomacromol 16:2427–2435

Garcia Calvo-Flores F, Dobado JA (2010) Lignin as renewable raw material. Chemsuschem 3:1227–1235

Gu J, Hsieh YL (2015) Surface and structure characteristics, self-assembling, and solvent compatibility of holocellulose nanofibrils. ACS Appl Mater Interfaces 7:4192–4201

Ha D, Fang Z, Zhitenev NB (2018) Paper in electronic and optoelectronic devices. Adv Electron Mater 4:1700593

Habibi Y (2014) Key advances in the chemical modification of nanocelluloses. Chem Soc Rev 43:1519–1542

Henriksson M, Berglund LA, Isaksson P, Lindstrom T, Nishino T (2008) Cellulose nanopaper structures of high toughness. Biomacromol 9:1579–1585

Horseman T, Tajvidi M, Diop CIK, Gardner DJ (2017) Preparation and property assessment of neat lignocellulose nanofibrils (LCNF) and their composite films. Cellulose 24:2455–2468

Hsieh MC, Koga H, Suganuma K, Nogi M (2017) Hazy transparent cellulose nanopaper. Sci Rep 7:41590

Hu S, Gu J, Jiang F, Hsieh YL (2016) Holistic rice straw nanocellulose and hemicelluloses/lignin composite films. ACS Sustain Chem Eng 4:728–737

Hu W, Chen G, Liu Y, Liu Y, Li B, Fang Z (2018) Transparent and hazy all-cellulose composite films with superior mechanical properties. ACS Sustain Chem Eng 6:6974–6980

Juzeniene A, Brekke P, Dahlback A, Andersson-Engels S, Reichrath J, Moan K, Holick MF, Grant WB, Moan J (2011) Solar radiation and human health. Rep Prog Phys 74:066701

Klemm D, Kramer F, Moritz S, Lindstrom T, Ankerfors M, Gray D, Dorris A (2011) Nanocelluloses: a new family of nature-based materials. Angew Chem Int Ed 50:5438–5466

Koga H, Nogi M, Komoda N, Thi Thi N, Sugahara T, Suganuma K (2014) Uniformly connected conductive networks on cellulose nanofiber paper for transparent paper electronics. Npg Asia Mater 6:e93

Lawoko M, Henriksson G, Gellerstedt G (2005) Structural differences between the lignin-carbohydrate complexes present in wood and in chemical pulps. Biomacromol 6:3467–3473

Leijonmarck S, Cornell A, Lindbergh G, Wagberg L (2013) Single-paper flexible Li-ion battery cells through a paper-making process based on nano-fibrillated cellulose. J Mater Chem A 1:4671–4677

Li X, Zhang X, Wang N, Chang H, Wang Y, Zhang Z (2019) Range-broadening ultraviolet-blocking regulation of cellulose nanopaper via surface self-absorption with poly(-methyl methacrylate)/avobenzone. ACS Appl Polym Mater 1:2981–2989

Mahpeykar SM, Zhao Y, Li X, Yang Z, Xu Q, Lu ZH, Sargent EH, Wang X (2017) Cellulose nanocrystal: polymer hybrid optical diffusers for index-matching-free light management in optoelectronic devices. Adv Opt Mater 5:1700430

Malucelli LC, Matos M, Jordao C, Lacerda LG, Carvalho Filho MAS, Magalhaes WLE (2018) Grinding severity influences the viscosity of cellulose nanofiber (CNF) suspensions and mechanical properties of nanopaper. Cellulose 25:6581–6589

Mishra RK, Sabu A, Tiwari SK (2018) Materials chemistry and the futurist eco-friendly applications of nanocellulose: status and prospect. J Saudi Chem Soc 22:949–978

Nair SS, Yan N (2015) Effect of high residual lignin on the thermal stability of nanofibrils and its enhanced mechanical performance in aqueous environments. Cellulose 22:3137–3150

Nemoto T, Konishi G, Tojo Y, Funaoka M (2010) Development of lignin as a transparent resin: evaluation of thermal and optical properties of alkoxylated lignophenols. Polym J 42:896–900

Nguyen KH, Chollet-Krugler M, Gouault N, Tomasi S (2013) UV-protectant metabolites from lichens and their symbiotic partners. Nat Prod Rep 30:1490–1508

Niskanen I, Suopajarvi T, Liimatainen H, Fabritius T, Heikkila R, Thungstrom G (2019) Determining the complex refractive index of cellulose nanocrystals by combination of Beer-Lambert and immersion matching methods. J Quant Spectrosc Radiat Transfer 235:1–6

Peng F, Ren JL, Xu F, Bian J, Peng P, Sun RC (2009) Comparative study of hemicelluloses obtained by graded ethanol precipitation from sugarcane bagasse. J Agric Food Chem 57:6305–6317

Rojo E, Peresin MS, Sampson WW, Hoeger IC, Vartiainen J, Laine J, Rojas OJ (2015) Comprehensive elucidation of the effect of residual lignin on the physical, barrier, mechanical and surface properties of nanocellulose films. Green Chem 17:1853–1866

Ruiz HA, Cerqueira MA, Silva HD, Rodriguez-Jasso RM, Vicente AA, Teixeira JA (2013) Biorefinery valorization of autohydrolysis wheat straw hemicellulose to be applied in a polymer-blend film. Carbohydr Polym 92:2154–2162

Sadeghifar H, Venditti R, Jur J, Gorga RE, Pawlak JJ (2017) Cellulose-lignin biodegradable and flexible UV protection film. ACS Sustain Chem Eng 5:625–631

Schroeter J, Felix F (2005) Melting cellulose. Cellulose 12:159–165

Spence KL, Venditti RA, Habibi Y, Rojas OJ, Pawlak JJ (2010) The effect of chemical composition on microfibrillar cellulose films from wood pulps: mechanical processing and physical properties. Bioresour Technol 101:5961–5968

Svard A, Brannvall E, Edlund U (2015) Rapeseed straw as a renewable source of hemicelluloses: extraction, characterization and film formation. Carbohydr Polym 133:179–186

Tang H, Butchosa N, Zhou Q (2015) A transparent, hazy, and strong macroscopic ribbon of oriented cellulose nanofibrils bearing poly(ethylene glycol). Adv Mater 27:2070–2076

Tao J, Fang Z, Zhang Q, Bao W, Zhu M, Yao Y, Wang Y, Dai J, Zhang A, Leng C, Henderson D, Wang Z, Hu L (2017) Super-clear nanopaper from agro-industrial waste for green electronics. Adv Electron Mater 3:1600539

Tarres Q, Vanesa Ehman N, Evangelina Vallejos M, Cristina Area M, Delgado-Aguilar M, Mutje P (2017) Lignocellulosic nanofibers from triticale straw: the influence of hemicelluloses and lignin in their production and properties. Carbohydr Polym 163:20–27

Velasquez-Cock J, Ganan P, Posada P, Castro C, Serpa A, Gomez HC, Putaux JL, Zuluaga R (2016) Influence of combined mechanical treatments on the morphology and structure of cellulose nanofibrils: thermal and mechanical properties of the resulting films. Ind Crops Prod 85:1–10

Wagberg L, Decher G, Norgren M, Lindstroem T, Ankerfors M, Axnaes K (2008) The build-up of polyelectrolyte multilayers of microfibrillated cellulose and cationic polyelectrolytes. Langmuir 24:784–795

Wang Q, Du H, Zhang F, Zhang Y, Wu M, Yu G, Liu C, Li B, Peng H (2018) Flexible cellulose nanopaper with high wet tensile strength, high toughness and tunable ultraviolet blocking ability fabricated from tobacco stalk via a sustainable method. J Mater Chem A 6:13021

Xu J, Krietemeyer EF, Boddu VM, Liu SX, Liu WC (2018) Production and characterization of cellulose nanofibril (CNF) from agricultural waste corn stover. Carbohydr Polym 192:202–207

Yagyu H, Saito T, Isogai A, Koga H, Nogi M (2015) Chemical modification of cellulose nanofibers for the production of highly thermal resistant and optically transparent nanopaper for paper devices. ACS Appl Mater Interfaces 7:22012–22017

Yang X, Berthold F, Berglund LA (2018) Preserving cellulose structure: delignified wood fibers for paper structures of high strength and transparency. Biomacromol 19:3020–3029

Yang W, Jiao L, Liu W, Dai H (2019) Manufacture of highly transparent and hazy cellulose nanofibril films via coating TEMPO-Oxidized wood fibers. Nanomaterials 9:107

Zhang Z, Chang H, Xue B, Han Q, Lu X, Zhang S, Li X, Zhu X, Wong W, Li K (2017) New transparent flexible nanopaper as ultraviolet filter based on red emissive Eu(III) nanofibrillated cellulose. Opt Mater 73:747–753

Zhang H, Shi L, Feng X (2018) Use of chitosan to reinforce transparent conductive cellulose nanopaper. J Mater Chem C 6:242–248

Zhang S, Liu G, Chang H, Li X, Zhang Z (2019a) Optical haze nanopaper enhanced ultraviolet harvesting for direct soft-fluorescent emission based on lanthanide complex assembly and oxidized cellulose nanofibrils. ACS Sustain Chem Eng 7:9966–9975

Zhang Z, Song F, Zhang M, Chang H, Zhang X, Li X, Zhu X, Lv X, Wang Y, Li K (2019b) Cellulose nanopaper with controllable optical haze and high efficiency ultraviolet blocking for flexible optoelectronics. Cellulose 26:2201–2208

Zhu H, Xiao Z, Liu D, Li Y, Weadock NJ, Fang Z, Huang J, Hu L (2013) Biodegradable transparent substrates for flexible organic-light-emitting diodes. Energy Environ Sci 6:2105–2111